ADVANCED MATERIALS
www.advmat.de

Highly Efficient Thermally Activated Delayed Fluorescence via J-Aggregates with Strong Intermolecular Charge Transfer

Jie Xue, Qingxin Liang, Rui Wang, Jiayue Hou, Wenqiang Li, Qian Peng, Zhigang Shuai, and Juan Qiao**

The development of high-efficiency and low-cost organic emissive materials and devices is intrinsically limited by the energy-gap law and spin statistics, especially in the near-infrared (NIR) region. A novel design strategy is reported for realizing highly efficient thermally activated delayed fluorescence (TADF) materials via J-aggregates with strong intermolecular charge transfer (CT). Two organic donor–acceptor molecules with strong and planar acceptor are designed and synthesized, which can readily form J-aggregates with strong intermolecular CT in solid states and exhibit wide-tuning emissions from yellow to NIR. Experimental and theoretical investigations expose that the formation of such J-aggregates mixes Frenkel excitons and CT excitons, which not only contributes to a fast radiative decay rate and a slow nonradiative decay rate for achieving nearly unity photoluminescence efficiency in solid films, but significantly decreases the energy gap between the lowest singlet and triplet excited states (≈0.3 eV) to induce high-efficiency TADF even in the NIR region. These organic light-emitting diodes exhibit external quantum efficiencies of 15.8% for red emission and 14.1% for NIR emission, which represent the best result for NIR organic light-emitting diodes (OLEDs) based on TADF materials. These findings open a new avenue for the development of high-efficiency organic emissive materials and devices based on molecular aggregates.

Organic light-emitting diodes (OLEDs) have been verified as the next generation display and lighting technology with advantages of high flexibility, energy conservation, ultrathinness, and light weight.[1–3] Generally, electrically injected free carriers in OLEDs recombine to generate singlet and triplet excitons in an expected ratio of 1:3 according to spin statistics,[4] and then radiative excitons produce light. Accordingly, highly efficient OLEDs rely on both the efficient harvest of normally nonradiative triplet excitons and the efficient transformation of radiative excitons into photons. To date, great breakthroughs have been made mainly focusing on overcoming the limitation imposed by normally nonradiative triplet excitons, including highly efficient phosphorescent OLEDs based on noble-metal complexes,[5,6] fluorescent OLEDs based on organic emitters with p-type delayed fluorescence and today's popular thermally activated E-type delayed fluorescence (TADF),[7–10] and recently reported radical-based OLEDs with doublet emission.[11,12] For purely organic emitters with cost advantage in comparison to noble-metal complexes, small energy gaps (ΔE_{ST}) between the lowest singlet (S_1) and triplet (T_1) excited states can increase reverse intersystem crossing rate constants (k_{RISC}) from T_1 to S_1 and induce effective TADF,[10,13] thereby harnessing triplet excitons and realizing unity exciton utilizing efficiency. In single organic molecules, small ΔE_{ST} can be achieved by minimizing the overlap of highest occupied molecular orbitals (HOMO) and lowest unoccupied molecular orbitals (LUMO),[13] which inevitably would lead to small transition dipole moments (M) and therefore small oscillator strengths and radiative decay rate constants (k_r).[14] Consequently, it is a dilemma to achieve small ΔE_{ST} and large k_r simultaneously in single organic molecules.

During the transformation of radiative excitons into photons, the photoluminescence (PL) quantum yields (ϕ_{PL}) of emitters are crucial for electroluminescence (EL). Generally, ϕ_{PL} can be simply expressed as

$$\phi_{PL} = \frac{k_r}{k_r + k_{nr}} \tag{1}$$

$$k_r \propto A = \frac{\left(\Delta E_{opt}\right)^3}{3\pi\varepsilon_0 c^3 \hbar^4} |M|^2 \tag{2}$$

$$k_{nr} \propto \alpha \exp\left(-\beta \Delta E_{opt}\right) \tag{3}$$

Dr. J. Xue, Q. Liang, R. Wang, J. Hou, W. Li, Prof. Z. Shuai, Dr. J. Qiao
Key Lab of Organic Optoelectronics and Molecular Engineering
of Ministry of Education
Department of Chemistry
Tsinghua University
Beijing 100084, P. R. China
E-mail: qjuan@mail.tsinghua.edu.cn
Dr. J. Xue, Dr. J. Qiao
Center for Flexible Electronics Technology
Tsinghua University
Beijing 100084, P. R. China
Dr. Q. Peng
Key Laboratory of Organic Solids
Institute of Chemistry
Chinese Academy of Sciences
Beijing 100190, P. R. China
E-mail: qpeng@iccas.ac.cn
The ORCID identification number(s) for the author(s) of this article can be found under https://doi.org/10.1002/adma.201808242.

DOI: 10.1002/adma.201808242

without consideration of the molecular vibrations, where A is Einstein's A coefficient, k_{nr} is the nonradiative decay rate constant, α and β are constants, and ΔE_{opt} is optical energy gap.[15] From Equations (1)–(3), we can know that k_r is mainly controlled by M and ΔE_{opt}, and the k_{nr} always obeys the energy gap law,[15–17] exponentially increasing with the decrease of ΔE_{opt}. In visible region from blue to red, high ϕ_{PL} can be achieved by sophisticated molecular design on single organic molecules. However, the limited transition dipole moments generated in single organic molecules meet its Waterloo as the decrease of ΔE_{opt} into deep-red and near-infrared (NIR) region in accord to the energy gap law. Consequently, it is still a formidable challenge to develop highly efficient deep-red and NIR emissive materials and devices, though urgently needed for applications spanning from night-vision displays and information-secured devices to medical diagnostics and phototherapy.[18]

Beyond single organic molecule (monomer), ordered supramolecular self-assembly of monomers into aggregates would endow materials exceptional and intriguing merits such as high carrier and exciton transporting rate,[19] untralong exciton migration distance (over ten thousand monomer units),[19] significantly suppressed k_{nr},[20] and largely enhanced emission efficiency,[21,22] which would provide an alternative way to solve the inextricable problems encountered at the single-molecule level. Generally, effective intermolecular exciton coupling between monomers can lead to the formation of aggregates with exciton states split.[19,23] The energy diagram for the aggregate (taking dimer as an example) with inclined packing motifs is displayed in **Figure 1**a. According to the Frenkel exciton (FE) model established by Kasha et al.,[24,25] the splitting energy ($\Delta\varepsilon$) of exciton states in dimer with inclined packing motifs can be expressed as

$$\Delta\varepsilon = \frac{2|M|^2}{d_{c-c}^3}\left(1-3\cos^2\theta\right) \tag{4}$$

where M is the transition dipole moment of pristine exciton state, d_{c-c} is the intermolecular center-to-center distance, and θ is the slip angle of dimer. Accordingly, the splitting of pristine singlet exciton states in J-aggregates ($\theta < 54.7°$) can generate lower-energy and dipole-allowed exciton states with larger transition dipole moments,[24,25] while pristine triplet exciton states are almost unchanged due to vanishingly small transition dipole moments, thereby resulting in a substantial reduction of ΔE_{ST} (Figure 1b). Therefore, in principle, red-shifted absorption and emission spectra, larger M, and smaller ΔE_{ST} could be achieved simultaneously in J-aggregates, which is highly desired to realize highly efficient TADF especially in NIR region. As is known, the charge-transfer (CT) state is the most important character for typical TADF materials because it highly decreases the ΔE_{ST}. In addition, the intermolecular CT exciton (CTE) states generated in aggregates with strong intermolecular interaction could further stabilize the excited states.[26] Therefore, we here aim to realize highly efficient TADF materials via J-aggregates with strong intermolecular CT characteristics through molecular design, which would provide great potential to achieve highly efficient organic emissive materials and devices even in NIR region.

To obtain the desired J-aggregates, we designed two donor–acceptor type monomers, TPAAP and TPAAQ (**Figure 2**a), based on the planar and strong electron-drawing acceptors acenaphtho[1,2-*b*]pyrazine-8,9-dicarbonitrile (AP) and acenaphtho[1,2-*b*]quinoxaline-8,9-dicarbonitrile (AQ) and a strong electron-donating donor triphenylamine (TPA). Both TPAAP and TPAAQ were readily synthesized in three steps including bromination, palladium catalyzed Suzuki–Miyaura cross-coupling reaction, and dehydration cyclization reaction, and were fully characterized by ^{1}H-NMR spectroscopy, high-resolution mass spectrometry, and elemental analysis. Both TPAAP and TPAAQ exhibit good thermal stabilities with high decomposition temperatures (T_d, corresponding to 5% weight loss) of 335 and 382 °C and high glass transition temperatures (T_g) of 115 and 136 °C (Figure S1, Supporting Information), respectively.

Single crystals of TPAAP and TPAAQ were readily obtained by temperature gradient vacuum sublimation. TPAAP and TPAAQ monomers in crystalline states possess relatively planar structures with large ground-state permanent dipole

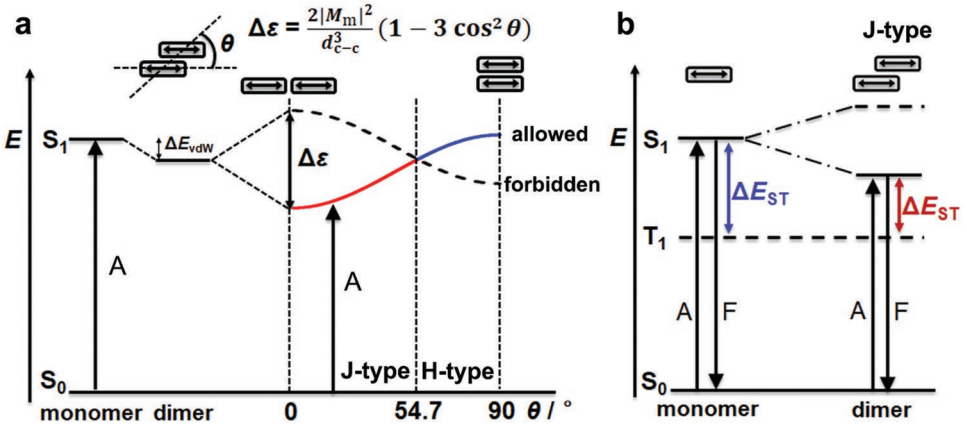

Figure 1. a) A schematic illustration for energy diagram of aggregated dimers (represented by gray rectangles) with coplanar transition dipoles inclined to interconnected axis by angle θ.[24,25] Double arrows represent the polarization axis for the molecular electronic transition considered. A = absorption, ΔE_{vdW} = difference in van der Waals interaction energies between ground and excited states. b) Schematic energy level diagram showing the evolution of S_1 and T_1 in J-aggregates without consideration of ΔE_{vdW}. A = absorption and F = fluorescence.

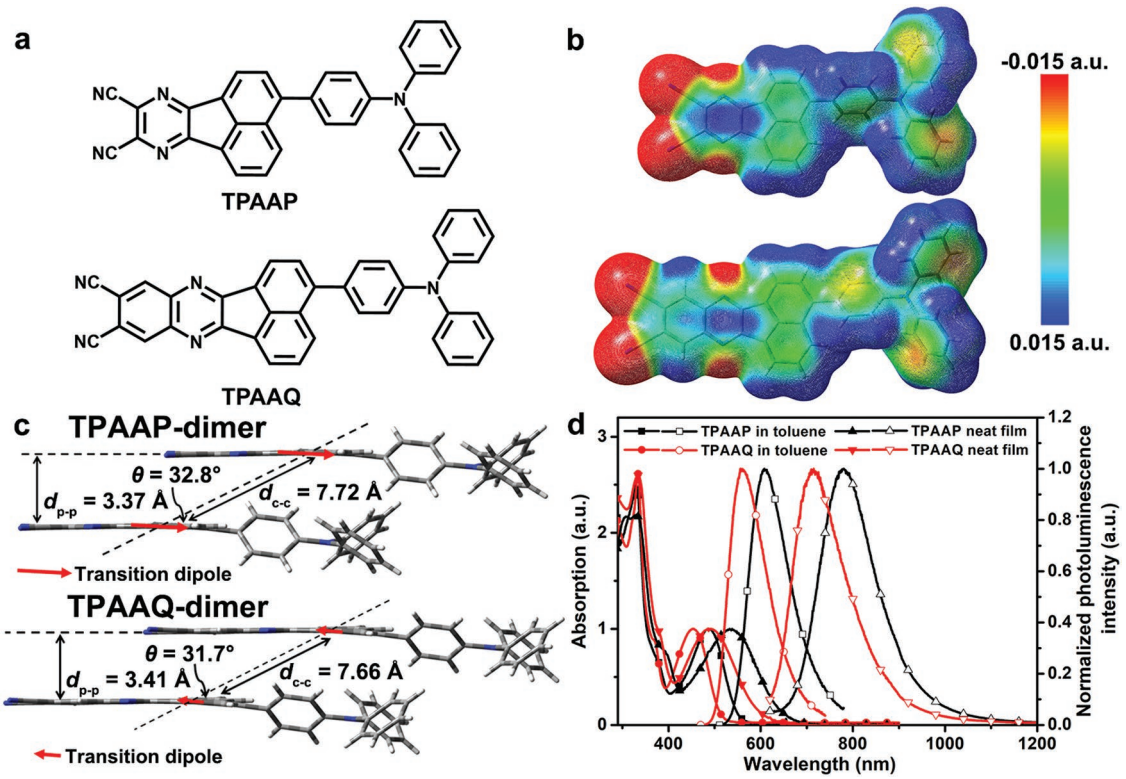

Figure 2. a) Chemical structures of TPAAP and TPAAQ. b) Electrostatic potential maps of TPAAP (top) and TPAAQ (bottom) in ground states with an isodensity surface of 0.005. c) Packing motifs of aggregated dimers of TPAAP and TPAAQ with transition dipoles of S_1 denoted as red arrows. The transition dipoles of S_1 were obtained by the time-dependent density functional theory approach at the level of TD/B3LYP/6-31G(d). d) Absorption (solid symbol) and PL (open symbol) spectra of TPAAP and TPAAQ in toluene and neat solid films.

moments (13.5 and 14.3 Debye, respectively). As shown in electrostatic potential maps (Figure 2b), the nitrile groups and nitrogen atoms in AP and AQ subunits have negative electrostatic potential while the other parts have neutral and positive potential, which leads to an inclined (staircase) molecular packing with electronegative parts close to electropositive parts in crystalline states as anticipated (Figure 2c). The intermolecular plane-to-plane distances (d_{p-p}) and center-to-center distances (d_{c-c}) are 3.37 and 7.72 Å for TPAAP and 3.41 and 7.66 Å for TPAAQ, respectively. Angles between the transition dipoles of S_1 states and the interconnected axis are 32.8° for TPAAP and 31.7° for TPAAQ, which are much smaller than the critical value of 54.7° and in favor of the formation of J-aggregates.[25] Furthermore, this J-type inclined packing extends in the aggregated polymers of TPAAP and TPAAQ in crystalline states (Figure S5, Supporting Information).

Photophysical properties of TPAAP and TPAAQ were investigated in dilute solutions. In toluene, both TPAAP and TPAAQ exhibit two major absorption bands (Figure 2d). The intense absorption bands at around 330 nm are ascribed to the localized π–π^* transitions of the conjugated skeletons, and the moderate absorption bands over 400 nm are assigned to the intramolecular CT transitions with peaks at 487 nm for TPAAP and 454 nm for TPAAQ. Compared to TPAAP, the extended π-conjunction in the acceptor segment of TPAAQ elevates the LUMO energy level (Figure S6, Supporting Information), thus leading to the hypsochromic shift of intramolecular CT absorption band. In oxygen-free toluene at room temperature, TPAAP displays an orange–red emission (λ_{max} = 609 nm) with a high ϕ_{PL} value of 97.3 ± 1.7% and a short lifetime of 6.90 ns (Figure S7, Supporting Information), and TPAAQ shows a yellow emission (λ_{max} = 560 nm) with a high ϕ_{PL} value of 93.0 ± 2.8% and a short lifetime of 4.91 ns. Notably, no delayed fluorescence was detected for both TPAAP and TPAAQ in oxygen-free toluene. Values of ΔE_{ST} are 0.19 and 0.33 eV for TPAAP and TPAAQ in toluene solutions (Figure S8, Supporting Information), respectively. As the variation of solvents' polarity, their PL spectra exhibit strong solvatochromic effects indicating the intramolecular CT nature of their emissions, while their absorption spectra were slightly affected (Figure S9, Supporting Information).

Most notably, in aggregation state, the neat films of TPAAP and TPAAQ exhibit significantly red-shifted PL spectra falling in NIR region (Figure 2d) with emission maxima at 777 nm for TPAAP and 716 nm for TPAAQ and good ϕ_{PL} values of 20.3 ± 2.5% and 16.3 ± 1.6%, respectively. Also, their neat films demonstrate largely red-shifted CT absorption bands with maxima peaks at 538 and 491 nm for TPAAP and TPAAQ, respectively. Interestingly, single crystals of TPAAP and TPAAQ exhibit exceptionally red-shifted absorption spectra with unusual absorption platform even extending to about 800 and 750 nm (Figure S10, Supporting Information), respectively. The substantially red-shifted absorptions of TPAAP and TPAAQ in neat films and single crystals are full of suggestions for the

formation of J-aggregates with intermolecular CT character in the solid states. The absorption bands of TPAAP and TPAAQ in tetrahydrofuran–water mixtures show abrupt large red-shifts with the increase of water volume fractions from 60% to 70%, also providing the evidence for the formation of J-aggregates as the aggregation of monomers (Figure S11, Supporting Information).

To track the evolution process of the J-aggregates, we studied the absorption and fluorescence spectra of the doped films with TPAAP or TPAAQ in 2,2′,2″-(1,3,5-benzinetriyl)-tris(1-phenyl-1-*H*-benzimidazole) (TPBi) at different weight concentrations from 0.1 to 100 wt%. As shown in **Figure 3** and Figure S14 in the Supporting Information, the low-energy CT absorption bands of TPAAP and TPAAQ exhibit progressive red-shift as the increase of doping concentrations, manifesting the participation of stronger and stronger intermolecular interaction even intermolecular electronic transitions in J-aggregates. The 0.1 wt% doped films of TPAAP:TPBi and TPAAQ:TPBi exhibit orange and greenish–yellow emissions with peak wavelengths at 597 and 538 nm, respectively, which are similar to aforementioned monomers' emissions in dilute toluene solutions. There are rapid red-shifts of the PL into NIR region (λ_{max} = 705 nm) for TPAAP and red region (λ_{max} = 642 nm) for TPAAQ as the doping concentrations increase from 0.1 to 15 wt%, and then slow red-shifts with the further increase of doping concentrations from 15 to 100 wt%. Accordingly, the S_1

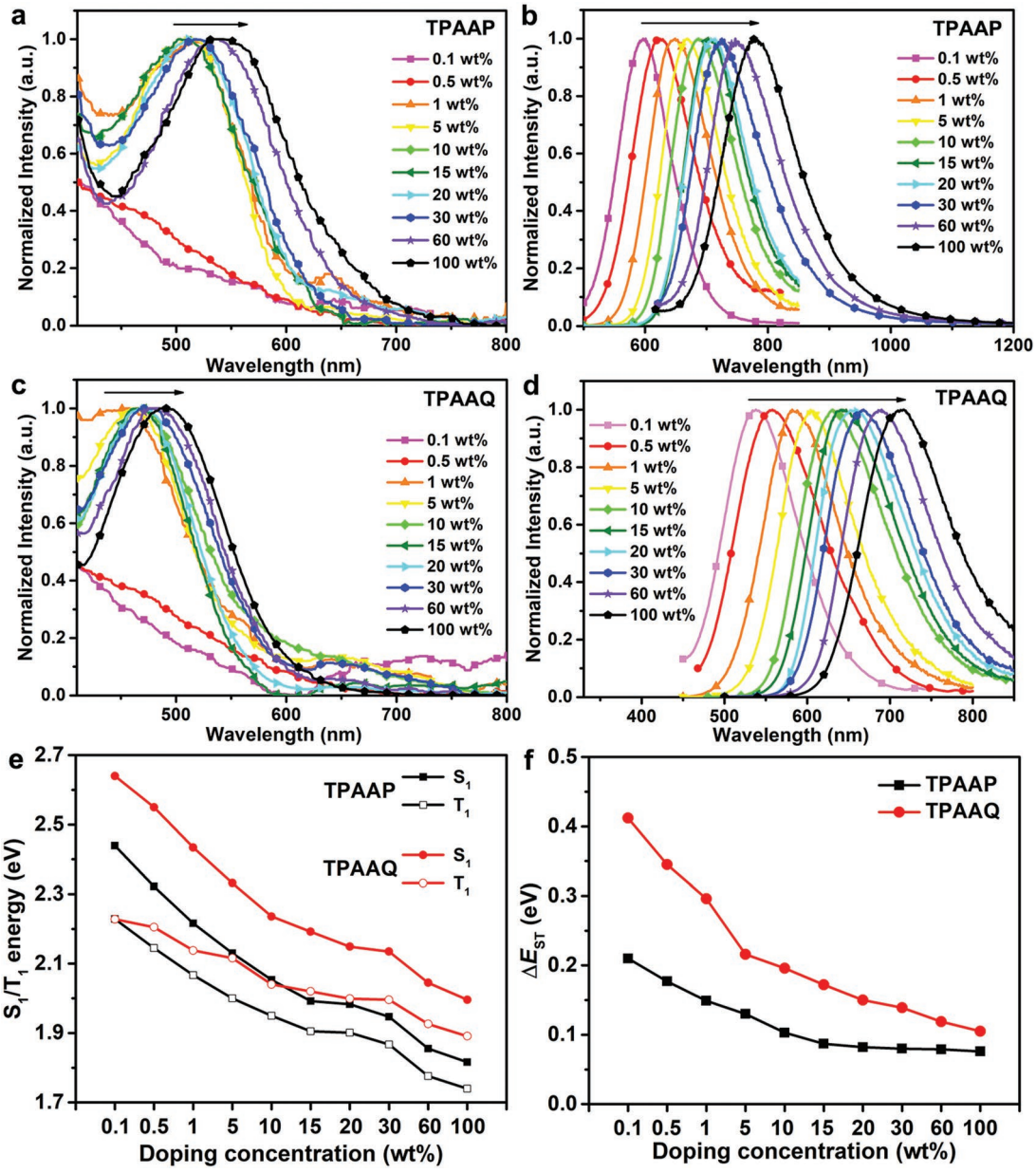

Figure 3. Absorption spectra of a) TPAAP and c) TPAAQ in solid films with TPBi as host at various doping concentrations. PL spectra of b) TPAAP and d) TPAAQ in solid films with TPBi as host at various doping concentrations at room temperature. e) Excited-state energies and f) ΔE_{ST} values of TPAAP and TPAAQ in a TPBi host matrix at various doping concentrations.

energies of TPAAP and TPAAQ exhibit large reductions of up to 0.623 and 0.644 eV from 2.439 and 2.640 eV to 1.816 and 1.996 eV (Figure 3e and Tables S2 and S3, Supporting Information), respectively. Such large declines of S_1 energies could be explained by the synergistic effect of the transformation of exciton states due to the formation of J-aggregates, the van der Waals interaction including π–π interactions between adjacent molecules and the self-polarization–induced solid-state solvation effect caused by larger ground-state permanent dipole moments of dyes compared with TPBi (Table S4, Supporting Information).[25,27] Also, the doped films with TPAAP or TPAAQ in poly(methyl methacrylate) (PMMA) display similar gradually red-shifted absorption and fluorescence (Figure S15, Supporting Information).

In addition, both TPAAP and TPAAQ doped films display gradually red-shifted phosphorescence spectra with the increase of doping concentrations from 0.1 to 100 wt%, demonstrating substantial reductions of their T_1 energies of 0.489 and 0.337 eV from 2.229 and 2.228 eV to 1.740 and 1.891 eV (Figure 3e, Tables S2 and S3, Supporting Information), respectively. Such large reductions of T_1 energies indicate the existence of Dexter energy transfer or CT between dyes in the solid state.[28,29] To note, although TPAAP and TPAAQ give nearly identical T_1 energies in TPBi host at low doping concentration of 0.1 wt%, the T_1 energy of TPAAP exhibits a larger reduction as the increase of doping concentration than that of TPAAQ. Based on the energy levels of S_1 and T_1 states, ΔE_{ST} of TPAAP and TPAAQ in solid films with TPBi as host were obtained, which demonstrate gradual reductions from 0.210 and 0.412 eV to 0.076 and 0.105 eV as the increase of doping concentrations from 0.1 to 100 wt% (Figure 3f), respectively.

As expected, the intriguing TADF is induced and enhanced for the TPAAP and TPAAQ in the solid films (**Figure 4**). For TPAAP:TPBi and TPAAQ:TPBi doped films with low doping concentration of 0.1 wt%, their transient PL spectra at room temperature show double-exponential decays with short average lifetimes of 6.39 and 4.35 ns (Tables S2 and S3, Supporting Information) and their temperature dependences show the absence of the TADF (Figures S18 and S22, Supporting Information), which could be ascribed to the large ΔE_{ST} values of TPAAP and TPAAQ monomers. As the increase of doping concentrations, the ΔE_{ST} values present gradual reductions to 0.149 and 0.296 eV for 1 wt% doped films (Tables S2 and S3, Supporting Information), and further to 0.103 and 0.196 eV for 10 wt% doped films, finally to 0.076 and 0.105 eV for the neat films of TPAAP and TPAAQ, respectively. It is easily understood that the intermolecular interaction accordingly increases with the increase of doping concentration. As a result, the J-type aggregates gradually form and their CT character becomes more and more remarkable, which lead to the decrease of ΔE_{ST}. For the 1 wt% doped films of TPAAP:TPBi and TPAAQ:TPBi, the transient PL spectra demonstrate double-exponential decays and the average delayed fluorescence lifetimes as long as 5.5 and 35.7 ms, respectively. With the increase of the doping concentrations, the average delayed fluorescence lifetimes decrease gradually. And for neat films of TPAAP and TPAAQ, the average lifetimes remarkably reduce to 10.4 and 8.1 µs (Figures S19 and S23, Supporting Information), respectively, which is mainly ascribed to the largely enhanced reverse intersystem crossing rate constants k_{RISC} due to the substantial reduction of ΔE_{ST}. The k_{RISC} values are significantly increased from 1.73×10^2 and 2.51×10^2 s^{-1} for 1 wt% doped films to 3.79×10^3 and 3.27×10^4 s^{-1} for the neat films of TPAAP and TPAAQ (Tables S2 and S3, Supporting Information), respectively.

As the doping concentrations increase, ϕ_{PL} of TPAAP:TPBi and TPAAQ:TPBi doped films display rapid increases in the range of 0.1–1 wt% with maxima values of 97.7 ± 1.8% (1 wt% TPAAP:TPBi film) and 94.6 ± 2.6% (1 wt% TPAAP:TPBi film), and then gradually decreases in the range of 1–100 wt% (Figure 4e,f, and Tables S2 and S3, Supporting Information), which is much better than recently reported outstanding NIR boron difluoride curcuminoid derivative at the same doping concentration.[30] Although J-aggregation have been reported to enlarge M and k_r,[19] the k_r of TPAAP and TPAAQ did not display the expected increase with the increase in doping concentration, but a gradual decrease (Tables S2 and S3, Supporting Information), which could be ascribed to the largely reduced ΔE_{opt} (see Equation (2)), solid-state solvation effect, and the participation of CTE states.[27,31] To note, relatively high k_r values (over 1×10^8 s^{-1}) can be retained for TPAAP and TPAAQ as the doping concentrations increase from 0.1 to 1 wt% even along with reductions of ΔE_{opt} values by 0.2 eV. More importantly, the k_{nr} values of TPAAP and TPAAQ demonstrate slight decreases by about a tenfold rather than exponential increase with reductions of ΔE_{opt} values by 0.2 eV (Tables S2 and S3, Supporting Information) as the doping concentrations increase from 0.1 to 1 wt%, which totally disobeys the well-known energy gap law. When the doping concentrations increase from 1 to 100 wt%, the k_{nr} values regain growth momentum mainly due to a combination of the aggregation-caused quenching and the reduction of ΔE_{opt}. For TPAAQ, although the ΔE_{opt} value was reduced by 0.64 eV with the increase inthe doping concentration in films from 0.1 to 100 wt%, the k_{nr} value showed a small decrease from 8.59×10^6 to 2.46×10^6 s^{-1}, totally deviating from exponential increase tend. For TPAAP, a 0.62 eV reduction of ΔE_{opt} value only lead to a slight increase of k_{nr} value from 1.74×10^6 to 3.96×10^6 s^{-1}. Such abnormal photophysical behaviors could be attributed to the formation and population of J-aggregates with strong intermolecular CT, which efficiently alleviate the vibrational quenching and suppress the nonradiative transitions.[20,32]

To understand the mechanism of the unusual photophysical behaviors of TPAAP and TPAAQ, we theoretically investigated their electronic structures and excited states of monomer and dimer in gas phase and in solid phase by hybrid quantum mechanics (QM) and molecular mechanics (MM) method. The QM parts were calculated by using density function theory (DFT) and time- dependent DFT (TDDFT) with B3LYP/6-31G(d); and the solid-state environments were mimicked by considering the electrostatic interaction and the van der Waals interaction via the potential energy of universal force field (UFF). The FE model is generally used to describe the electronic excitations of organic aggregates when the hole–electron pair entirely locates on one molecule. Considering the exciton coupling interaction, the values of $\Delta\varepsilon/2$ were calculated to be –49.0 meV for S_1 of TPAAP and –8.2 and –79.8 meV for S_1 and S_2 of TPAAQ (TPAAQ monomer possess close lying S_1 and S_2, see

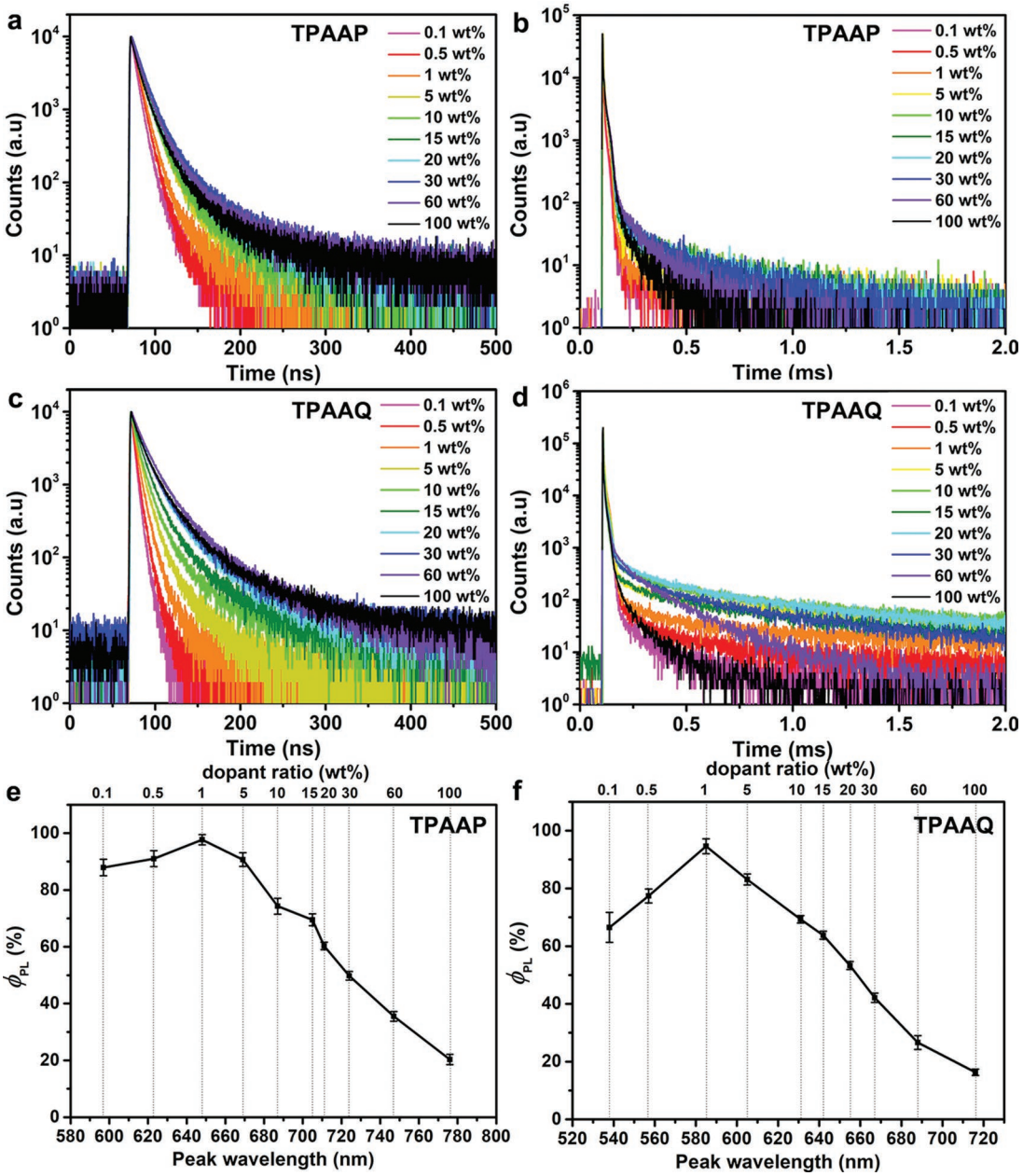

Figure 4. Transient PL decay curves of a,b) TPAAP and c,d) TPAAQ in solid films with TPBi as host at various doping concentrations at room temperature. ϕ_{PL} and emission peak wavelengths of e) TPAAP and f) TPAAQ in solid films with TPBi as host at various doping concentrations at room temperature.

Table S5 in the Supporting Information), respectively. Although a twice exciton splitting energy could be expected in aggregated polymer considering a nearest-neighbor approximation that each molecule in the aggregated polymer has two neighbors,[24] the stabilized energies in aggregated polymers calculated based on FE model are still much smaller than the aforementioned reductions of S_1 energies. Then the intermolecular CTE, whose hole–electron pair occupies adjacent molecules,[26] would be generated to further decrease the excited-state energy for both TPAAP and TPAAQ aggregates. The dimers are chosen from the nearest dimer in crystal structure to perform TDDFT calculations. From monomer to dimer in gas phase, the S_1 energies exhibited significant declines of 0.339 and 0.259 eV from 2.073 and 2.310 eV to 1.734 and 2.051 eV for TPAAP and TPAAQ (Table S5, Supporting Information), respectively, which are close to the experimental data. The T_1 energies demonstrated minor reductions from 1.836 and 2.000 eV to 1.726 and 1.986 eV for TPAAP and TPAAQ, respectively. Thus, the ΔE_{ST} reduce remarkably from 0.237 and 0.309 eV to 0.008 and 0.065 eV for TPAAP and TPAAQ, respectively, which could induce and enhance the intriguing TADF. Furthermore, the dimers in crystalline states demonstrate lower S_1 and T_1 energies (Table S6, Supporting Information) owing to the surrounding intermolecular interaction relative to that in gas

phase. As show in Table S6 in the Supporting Information, the S_1 energies calculated to be 1.609 and 2.016 eV and the T_1 energies calculated to be 1.568 and 1.881 eV for the dimers of TPAAP and TPAAQ in crystalline states based on the optimized ground geometries, respectively.

To more intuitively understand the nature of exciton states, natural transition orbital (NTO) analyses were carried out for the S_1 and T_1 excited states of the monomers and dimers for TPAAP and TPAAQ in gas phase (see **Figure 5**).[33] For the monomers of TPAAP and TPAAQ, their S_1 states are predominantly intramolecular CT in nature, while their T_1 states demonstrate a coexistence of local-excitation (LE) and intramolecular CT nature. In comparison, for the dimers of TPAAP and TPAAQ, their S_1 states both have a significant intermolecular CT character, which provides an important way to effectively stabilize the S_1 states. Therefore, in the case of TPAAP and TPAAQ aggregates, the S_1 states are assigned to mix the J-type FE and CTE. Although the CT nature is unfavorable for the electronic dipole transition owing to the separation of electron and hole in different molecule, the J-type FE could enhance the electronic dipole transition,[16] which contributes relatively large oscillator strengths for such J-aggregates. The oscillator strengths were calculated to be 0.0022 and 0.0010 for dimers of TPAAP and TPAAQ with ΔE_{ST} of only 0.008 and 0.065 eV (Table S5, Supporting Information), respectively, which are larger than typical single-molecule TADF materials with close ΔE_{ST}.[34,35] As for T_1 states of dimers, TPAAP is predominantly intermolecular CT in nature, while TPAAQ is predominantly LE in nature with a small intermolecular CT contribution. As a result, the T_1 energy shows a larger decline for TPAAP from monomer to dimer than that of TPAAQ. Also, the M062X functional with long-range correction were used to perform the calculations on the ground and excited electronic states of TPAAP and TPAAQ with 6-31G(d) basis set, which are basically consistent with the theoretical results carried out at the level of B3LYP/6-31G(d) (see Supporting Information).

Based on the result and discussion above, a mixed FE-CTE model is therefore proposed to describe the exciton states of TPAAP and TPAAQ aggregates (Figure 5c). In the mixed FE-CTE model, the aggregate's excited states are ascribed to the mixture of FE states and CTE states. On the one hand, the FE states

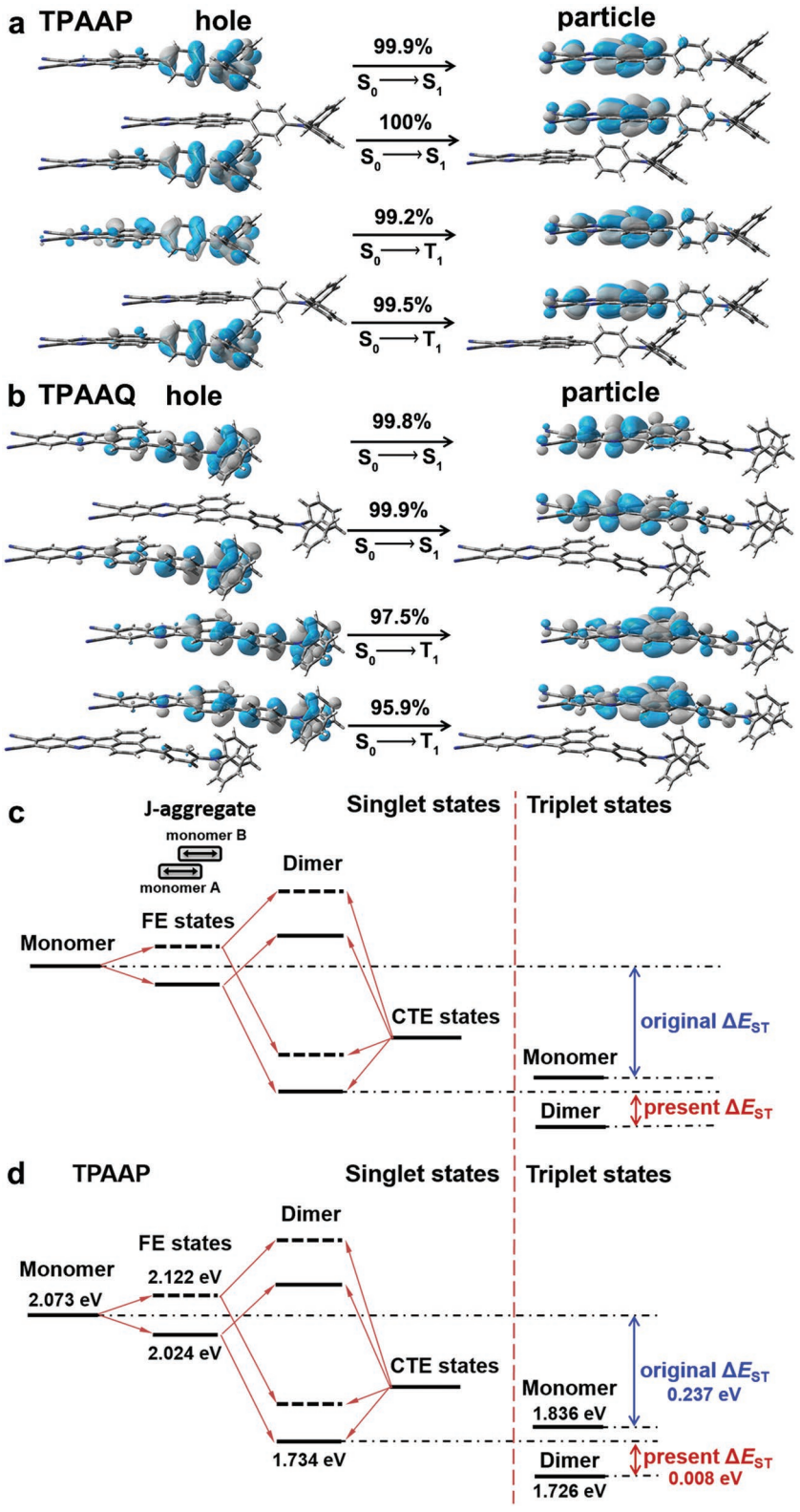

Figure 5. Natural transition orbitals of S_1 and T_1 states for the monomers and dimers of a) TPAAP and b) TPAAQ derived from single-crystal diffraction data carried out at the level of B3LYP/6-31G(d) in gas phase. c) The schematic energy diagram for the exciton states of J-type dimers based on a mixed FE-CTE model. d) The schematic energy diagram for the exciton states of TPAAP dimers based on a mixed FE-CTE model with energy levels of exciton states denoted.

are generated owing to the exciton coupling interaction between the monomers, and the lower-energy FE state is dipole-allowed in the J-type dimer according to FE model. On the other hand, the CTE is produced owing to the strong intermolecular interaction between donor and accepter from neighboring molecules. Then, the further couplings between FE and CTE lead to four new mixed states coming into being. Two exciton states are dipole-allowed exciton states with CT nature and the others are dipole-forbidden ones with CT nature. Herein, the lowest-energy exciton state is dipole-allowed FE with strong CT nature, which facilitates the radiative process and the generation of small ΔE_{ST} to obtain highly efficient TADF. And based on aforementioned theoretical results carried out at the level of B3LYP/6-31G(d) in gas phase, the schematic energy diagram for the exciton states of TPAAP was plotted (Figure 5d).

To evaluate the electroluminescent performance of these J-aggregates, we fabricated OLEDs with multilayer configurations of indium tin oxide (ITO)/1,4,5,8,9,11-hexaazatriphenylene hexacarbonitrile (HATCN, 5 nm, hole-injecting layer)/*N*,*N*′-bis(naphthalen-1-yl)-*N*,*N*′-bis(phenyl)benzidine (NPB, 70 nm, hole transporting layer)/1,3-bis(*N*-carbazolyl)benzene (mCP, 5 nm) or 4,4′,4″-tris(carbazol-9-yl)triphenylamine (TCTA, 5 nm) (exciton blocking layer)/TPBi: *x* wt% TPAAP or TPAAQ (30 nm, emitting layer)/TPBi (40 nm, electron transporting layer)/LiF (1 nm, electron-injecting layer)/Al (150 nm). In red and deep-red regions, OLEDs with 5 wt% TPAAQ:TPBi (device AQ-5) and 10 wt% TPAAP:TPBi (device AP-10) as emitting layers (EMLs) and mCP as exciton blocking layers (EBLs) exhibited maximum external quantum efficiencies (EQEs) of 15.8% and 14.1% with EL peaks at 630 and 657 nm (**Figure 6**), respectively. To tune emission into NIR region and reduce the turn-on voltage, the concentrations of TPAAQ and TPAAP in EML were increased and mCP was replaced by another EBL material TCTA. Device AP-15 with 15 wt% TPAAP:TPBi as EML and TCTA as EBLs achieved a maximum EQE of 14.1% with EL peak at 700 nm. In addition, the nondoped devices AQ-100 and AP-100 with neat TPAAQ and TPAAP films as EMLs exhibited strong NIR emissions with maximum EQEs of 3.5% (711 nm) and 5.1% (765 nm), respectively. Interestingly, the efficiency roll-offs of these devices were alleviated with the increase in doping concentration in the EML, which consists well with the aforementioned decreased ΔE_{ST} and enhanced TADF in films with higher doping concentration. The outstanding EQEs of these OLEDs represent the best results for NIR emitting devices based on TADF materials (Figure 6c).[30,36–39]

In summary, we have proposed and verified a novel and universal strategy for organic dyes to simultaneously stabilize excited states, reduce the nonradiative decay rate, and induce highly efficient TADF even in NIR region through the formation of J-aggregates with strong intermolecular CT. The mixed Frenkel–CT exciton model was proposed to describe the unique photophysical behaviors of these aggregates. The significantly reduced ΔE_{ST} due to the formation of such J-aggregates provides a new strategy for organic fluorescent dyes to induce and enhance TADF and achieve highly efficient electroluminescence via the efficient harvest of the triplet excitons. Also, the formation of such J-aggregates provides a way to suppress the nonradiative transitions and develop highly efficient organic emissive materials even in NIR region. It is anticipated that the intriguing merits gifted by the formation of J-aggregates with strong intermolecular CT would inject new vitality into organic materials for diverse advanced applications in flexible and wearable organic optoelectronic devices, biological imaging, and other fields.

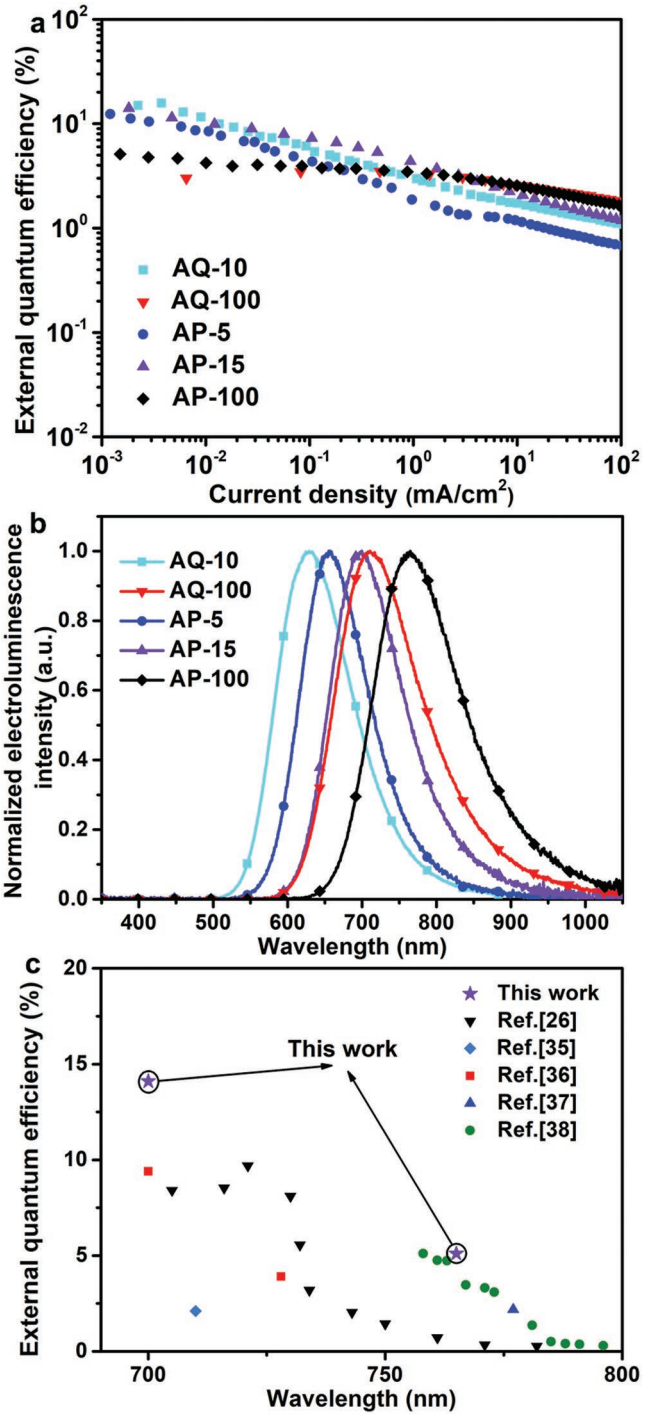

Figure 6. a) EQE as a function of current density. b) EL spectra at a voltage of 5.4 V for the devices AQ-10 and AP-5, and at a voltage of 3.2 V for the devices AP-15, AQ-100, and AP-100. c) Maximum EQE summary of the representative NIR-OLEDs based on TADF materials with emission peak from 700 to 800 nm.

Supporting Information

Supporting Information is available from the Wiley Online Library or from the author.

Acknowledgements

This work was supported by the National Key R&D Program of China (Grant Nos. 2016YFB0401003 and 2017YFA0204501), National Natural Science Foundation of China (Grant Nos. 51473086, 51773109, and 21788102), the National Key Basic Research and Development Program of China founded by MOST (No. 2015CB655002), the National Postdoctoral Program for Innovative Talents (Grant No. BX20180159), and Tsinghua University Initiative Scientific Research Program. The authors thank Professor Wanzhen Liang from College of Chemistry and Chemical Engineering, Xiamen University, for her stimulating discussion.

Conflict of Interest

The authors declare no conflict of interest.

Keywords

intermolecular charge transfer, J-aggregates, near-infrared emission, organic light-emitting diodes, thermally activated delayed fluorescence

Received: December 21, 2018
Revised: April 13, 2019
Published online: May 12, 2019

[1] C. Tang, S. VanSlyke, *Appl. Phys. Lett.* **1987**, *51*, 913.
[2] J. Kido, M. Kimura, K. Nagai, *Science* **1995**, *267*, 1332.
[3] J. A. Rogers, T. Someya, Y. Huang, *Science* **2010**, *327*, 1603.
[4] M. Segal, M. A. Baldo, R. J. Holmes, S. R. Forrest, Z. G. Soos, *Phys. Rev. B* **2003**, *68*, 075211.
[5] M. A. Baldo, D. F. O'Brien, Y. You, A. Shoustikov, S. Sibley, M. E. Thompson, S. R. Forrest, *Nature* **1998**, *395*, 151.
[6] C. Adachi, M. A. Baldo, M. E. Thompson, S. R. Forrest, *J. Appl. Phys.* **2001**, *90*, 5048.
[7] J. Kido, Y. Iizumi, *Appl. Phys. Lett.* **1998**, *73*, 2721.
[8] D. Kondakov, T. Pawlik, T. Hatwar, J. Spindler, *J. Appl. Phys.* **2009**, *106*, 124510.
[9] A. Endo, M. Ogasawara, A. Takahashi, D. Yokoyama, Y. Kato, C. Adachi, *Adv. Mater.* **2009**, *21*, 4802.
[10] H. Uoyama, K. Goushi, K. Shizu, H. Nomura, C. Adachi, *Nature* **2012**, *492*, 234.
[11] Q. Peng, A. Obolda, M. Zhang, F. Li, *Angew. Chem., Int. Ed.* **2015**, *54*, 7091.
[12] X. Ai, E. W. Evans, S. Dong, A. J. Gillett, H. Guo, Y. Chen, T. J. H. Hele, R. H. Friend, F. Li, *Nature* **2018**, *563*, 536.
[13] M. Y. Wong, E. Zysman-Colman, *Adv. Mater.* **2017**, *29*, 1605444.
[14] X.-K. Chen, Y. Tsuchiya, Y. Ishikawa, C. Zhong, C. Adachi, J.-L. Brédas, *Adv. Mater.* **2017**, *29*, 1702767.
[15] A. Tsuboyama, S. Okada, K. Ueno, in *Highly Efficient OLEDs with Phosphorescent Materials* (Ed: H. Yersin), Wiley-VCH Verlag GmbH & Co. KGaA, Weinheim, Germany **2008**, p. 163.
[16] W. Siebrand, *J. Chem. Phys.* **1967**, *47*, 2411.
[17] J. V. Caspar, T. J. Meyer, *J. Phys. Chem.* **1983**, *87*, 952.
[18] G. Qian, Z. Y. Wang, *Chem. – Asian J.* **2010**, *5*, 1006.
[19] F. Würthner, T. E. Kaiser, C. R. Saha-Möller, *Angew. Chem., Int. Ed.* **2011**, *50*, 3376.
[20] Z. An, C. Zheng, Y. Tao, R. Chen, H. Shi, T. Chen, Z. Wang, H. Li, R. Deng, X. Liu, W. Huang, *Nat. Mater.* **2015**, *14*, 685.
[21] S. Choi, J. Bouffard, Y. Kim, *Chem. Sci.* **2014**, *5*, 751.
[22] H. Fidder, J. Terpstra, D. A. Wiersma, *J. Chem. Phys.* **1991**, *94*, 6895.
[23] W. Li, Q. Peng, Y. Xie, T. Zhang, Z. Shuai, *Acta Chim. Sin.* **2016**, *74*, 902.
[24] E. G. McRae, M. Kasha, in *Physical Processes in Radiation Biology* (Eds: L. Augenstein, R. Mason, B. Rosenberg), Academic Press, New York, USA **1964**, p. 23.
[25] M. Kasha, H. R. Rawls, M. Ashraf El-Bayoumi, *Pure Appl. Chem.* **1965**, *11*, 371.
[26] F. Gao, W. Liang, Y. Zhao, *Sci. China: Chem.* **2010**, *53*, 297.
[27] C. F. Madigan, V. Bulović, *Phys. Rev. Lett.* **2003**, *91*, 247403.
[28] G. D. Scholes, *J. Phys. Chem.* **1996**, *100*, 18731.
[29] G. D. Scholes, R. D. Harcourt, K. P. Ghiggino, *J. Chem. Phys.* **1995**, *102*, 9574.
[30] D.-H. Kim, A. D'Aléo, X.-K. Chen, A. D. S. Sandanayaka, D. Yao, L. Zhao, T. Komino, E. Zaborova, G. Canard, Y. Tsuchiya, E. Choi, J. W. Wu, F. Fages, J.-L. Brédas, J.-C. Ribierre, C. Adachi, *Nat. Photonics* **2018**, *12*, 98.
[31] E. M. Kosower, H. Dodiuk, H. Kanety, *J. Am. Chem. Soc.* **1978**, *100*, 4179.
[32] K. Tuong Ly, R.-W. Chen-Cheng, H.-W. Lin, Y.-J. Shiau, S.-H. Liu, P.-T. Chou, C.-S. Tsao, Y.-C. Huang, Y. Chi, *Nat. Photonics* **2017**, *11*, 63.
[33] R. L. Martin, *J. Chem. Phys.* **2003**, *118*, 4775.
[34] Q. Zhang, H. Kuwabara, W. J. Potscavage, S. Huang, Y. Hatae, T. Shibata, C. Adachi, *J. Am. Chem. Soc.* **2014**, *136*, 18070.
[35] T. Takahashi, K. Shizu, T. Yasuda, K. Togashi, C. Adachi, *Sci. Technol. Adv. Mater.* **2014**, *15*, 034202.
[36] S. Wang, X. Yan, Z. Cheng, H. Zhang, Y. Liu, Y. Wang, *Angew. Chem., Int. Ed.* **2015**, *54*, 13068.
[37] C. Li, R. Duan, B. Liang, G. Han, S. Wang, K. Ye, Y. Liu, Y. Yi, Y. Wang, *Angew. Chem., Int. Ed.* **2017**, *56*, 11525.
[38] Y. Yuan, Y. Hu, Y.-X. Zhang, J.-D. Lin, Y.-K. Wang, Z.-Q. Jiang, L.-S. Liao, S.-T. Lee, *Adv. Funct. Mater.* **2017**, *27*, 1700986.
[39] H. Ye, D. H. Kim, X. Chen, A. S. D. Sandanayaka, J. U. Kim, E. Zaborova, G. Canard, Y. Tsuchiya, E. Y. Choi, J. W. Wu, F. Fages, J.-L. Brédas, A. D'Aléo, J.-C. Ribierre, C. Adachi, *Chem. Mater.* **2018**, *30*, 6702.

